Density profiles and substructure of dark matter halos: converging results at ultra-high numerical resolution.

S. Ghigna[1], B. Moore[1], F. Governato[2], G. Lake[3], T. Quinn[3], J. Stadel[3]

ABSTRACT

Can dissipationless N-body simulations be used to reliably determine the structural and substructure properties of dark matter halos? A large simulation of a galaxy cluster in a cold dark matter universe is used to increase the force and mass resolution of current "high resolution simulations" by almost an order of magnitude to examine the convergence of the important physical quantities. The cluster contains ~ 5 million particles within the final virial radius, $R_{vir} \simeq 2\,\mathrm{Mpc}$ (with $H_0 = 50\,\mathrm{Km\,s^{-1}\,Mpc^{-1}}$), and is simulated using a force resolution of 1.0 kpc ($\equiv 0.05\%$ of R_{vir}); the final virial mass is $4.3\,10^{14} M_\odot$, equivalent to a circular velocity $v_{circ} \equiv (GM/R)^{1/2} \simeq 1000\,\mathrm{km\,s^{-1}}$ at the virial radius. The central density profile has a logarithmic slope of -1.5, identical to lower resolution studies of the same halo, indicating that the profiles measured from simulations of this resolution have converged to the "physical" limit down to scales of a few kpc ($\sim 0.2\%$ of R_{vir}). Also the abundance and properties of substructure are consistent with those derived from lower resolution runs; from small to large galaxy scales ($v_{circ} > 100\,\mathrm{km\,s^{-1}}$, $m > 10^{11} M_\odot$), the circular velocity function and the mass function of substructures can be approximated by power laws with slopes ~ -4 and ~ -2 respectively. At the current resolution, overmerging — a numerical effect that leads to structureless virialized halos in low-resolution N-body simulations — seems to be globally unimportant for substructure halos with circular velocities $v_{circ} > 100\,\mathrm{km\,s^{-1}}$ ($\sim 10\%$ of the cluster's v_{circ}). We can identify subhalos orbiting in the very central region of the cluster ($R \lesssim 100$ kpc) and we can trace most of the cluster progenitors from high redshift to the present. The object at the cluster center (the dark matter analog of a cD galaxy) is assembled between $z = 3$ and $z = 1$ from the merging of a dozen halos with $v_{circ} \gtrsim 300\,\mathrm{km\,s^{-1}}$. Tidal stripping and halo-halo collisions decrease the mean circular velocity of the substructure halos by $\approx 20\%$ over a 5 billion year period. We use the sample of 2000 substructure halos to explore the possibility of biases using galactic tracers in clusters: the velocity dispersions of the halos globally agree with the dark matter within $\lesssim 10\%$, but the halos are spatially anti-biased, and in the very central region of the cluster ($R/R_{vir} < 0.3$), they show positive velocity bias ($b_v \equiv \sigma_{v3D,halos}/\sigma_{v3D,DM} \simeq 1.2$–$1.3$); however, this effect appears to depend on numerical resolution.

Subject headings: cosmology: theory – dark matter – large–scale structure of the Universe – galaxies: clusters – galaxies: halos – methods: numerical

[1]Physics Department, University of Durham, Durham City, UK

[2]Osservatorio di Brera-Merate, Milano, Italy

[3]Astronomy Department, University of Washington, Seattle, USA

1. Introduction

In hierachical cosmological scenarios galaxies and clusters form in virialized dark matter dominated halos that are assembled via merging and accretion of smaller structures (White & Rees 1978, Davis *et al* 1985; for a recent analysis, e.g. Tormen 1997, 1998). Until recently, to what extent the *subhalos* survive within the potential well

of the larger system has been largely uncertain, because cosmological N-body simulations were not able to resolve more than a handful of substructure halos (e.g. Carlberg 1994, Summers, Davis & Evrard 1995, Frenk *et al* 1996). Infalling subhalos are heated by tidal forces generated by the global potential and by mutual encounters and rapidly lose a large fraction of their masses; this is a physical effect but is greatly enhanced by limited numerical resolution. The finite resolution sets an upper limit to the potential depth of halos - large force softening or low numbers of particles per halo conspire to produce soft, diffuse substructure halos that are easily disrupted by tidal forces (Moore, Katz & Lake 1996) and lead to structureless virialised halos. This is the classic *overmerging* problem (White *et al* 1987).

Gas physics is not a solution; it is necessary to accurately reproduce the dynamics of the (dominant) dark matter component. It is now clear that mass and force resolution of the simulations are the key parameters for overcoming the overmerging problem (Moore, Katz & Lake 1996, Brainerd, Goldberg & Villumsen 1998, Moore *et al* 1998, Ghigna *et al* 1998, Tormen, Diaferio & Syers 1998, Klypin, Gottlöber, Kravtsov & Kokhlov 1999a, Okamoto & Habe 1999). Increased resolution leads to substructure halos (*subhalos* hereafter) with higher central densities, enabling them to survive. Halos extracted from large cosmological simulations and re-simulated (see next section) with $\sim 10^6$ particles and force resolution $\lesssim 0.01\%$ of the virial radius yield a wealth of substructure allowing a comparison between the mass and light distributions within clusters and galaxies (Ghigna *et al* 1998, hereafter G98; Okamoto & Habe 1999, Moore *et al* 1999a). Tormen, Diaferio & Syers (1998) have addressed the same issue using a sample of clusters simulated at lower resolution. High-resolution simulations of moderately large cosmological volumes that retain significant amounts of substructure within virialized halos have also become recently feasible (Klypin *et al* 1999a, hereafter KGKK; Klypin, Kravtsov, Valenzuela & Prada 1999b; Colín, Klypin, Kravtsov & Khokhlov 1999; Colín, Klypin & Kravtsov 1999; see also Kauffman *et al* 1999a, 1999b and Diaferio *et al* 1999). These latter approaches have the advantage of providing relatively large samples of dark matter halos representing clusters, groups or galaxies, but cannot detect systematic biases introduced by the limited resolution.

The central density profile of halos is also affected by numerical resolution. In order to compare the predictions of hierarchical models with observational data on the mass, light and X-ray profiles of clusters (e.g. Carlberg *et al* 1996, Carlberg, Yee & Ellingson 1997, Smail *et al* 1997, AbdelSalam, Saha & Williams 1998, Adami, Mazure, Katgert & Biviano 1998, Allen 1998, Markevitch, Vikhlin, Forman & Sarazin 1999), galaxy rotation curves (e.g. Moore 1994, Flores & Primack 1994, Moore *et al* 1999b and references therein), giant arc properties in gravitationally lensing clusters (e.g. Kneib *et al* 1996; also, Williams, Navarro & Bartelmann 1999, Flores, Maller & Primack 2000, Meneghetti *et al* 2000) or constraints on processes directly related to the nature of the dark matter, such as particle-particle annihilation rates (Calcaneo-Roldan & Moore, in preparation), it is important to resolve the central structure of dark matter halos. Using N-body simulations with $10^4 - 10^5$ particles per halo for the CDM models and its popular variants, Navarro, Frenk & White (1996, 1997) found that the profiles of isolated relaxed dark matter halos can be well described by a "universal" profile (NFW profile) from galactic to cluster scales; these results have been confirmed by other authors using simulations of comparable resolution — e.g Cole & Lacey 1996, Tormen, Bouchet & White 1996. However, improving the numerical resolution (Moore *et al* 1998) leads to profiles with central cusps significantly steeper than that of an NFW profile ($\rho(r) \propto r^{-1}$ for the latter); halos simulated with $\sim 10^6$ particles have profiles fit by the functional form $\rho(r) \propto [(r/r_s)^{1.5}(1 + (r/r_s)^{1.5})]^{-1}$ (Moore *et al* 1999b), which has a cusp $\rho(r) \propto r^{-1.5}$ as $r \to 0$. (In a recent analysis, Jing & Suto, 2000, find similar results for galaxies and groups, but shallower central profiles for a sample of clusters simulated in a ΛCDM cosmology; see our comments in § 4).

In this paper, we examine how much resolution per halo is required to make numerical effects negligible for various physical quantities and obtain robust results on the halo density profiles and the space, mass, velocity distribution of substructures. We perform one large (and expensive) simulation of a dark matter halo, taking the simulation originally analysed by Ghigna *et al* (1998; hereafter

G98) and increasing the force and mass resolution by almost an order of magnitude.

The plan of the paper is as follows: In §2, we describe the N-body simulations and, in § 3, the method used to identify the substructure halos. In § 4, we consider the issue of the typical density profile of isolated and substructure halos. Section 5 is devoted to the statisitcal properties of the substructure, the effects of resolution, evolution and environment. We study the distribution of their internal velocities and masses, their spatial distribution and whether they trace the mass, and also the issue of velocity bias. In § 7, we examine the relation between the cluster progenitor halos at high redshift and the substructure halos at the present epoch, and the formation of the central "cD" halo. We summarise the results and conclude in § 8.

2. The N–body simulations

Our aim is to achieve very high spatial and mass resolution within the dark halo of a cluster drawn from a "fair volume" of a standard CDM universe. To achieve such resolution, we initially perform a simulation of a large volume ($50\,h^{-1}$Mpc per side) of a CDM universe (normalised such that $\sigma_8 = 0.7$ and with the shape parameter $\Gamma = 0.5$ and $H_0 = 50\,\mathrm{Km\,s^{-1}\,Mpc^{-1}}$). The size of this box is nearly ten times the turnaround radius allowing the tidal field and hence infall pattern to be modelled correctly. We choose a cluster that is virialised by a redshift $z = 0$ and use a technique of "volume renormalization" to obtain higher resolution within the region of interest (see G98 and references therein). Our goal is to simulate the formation of this cluster such that $\sim 10^7$ particles lie within the turnaround radius at the final time. (Note that if we simulated the entire volume at this resolution we would need to use a total of 6×10^8 particles.) Beyond the turnaround region the mass resolution is decreased in a series of shells allowing us to reproduce the external tidal field correctly. The particle distribution is evolved using the high performance parallel treecode PKDGRAV, using periodic boundaries and a variable timestep scheme based upon the local acceleration (Quinn *et al* 1997, Wadsley, Quinn & Stadel 2000, in preparation). To maintain accurate forces when the mass distribution is fairly regular, from a redshift z=69 to z=2 we use an opening angle of 0.4 and we complete the simulation using an opening angle of 0.7. We expand the cell moments to hexadecapole order. The code uses a spline softening length such that the force is completely Newtonian at twice our quoted softening lengths. The time integration method is an adaptive implementation of the standard leapfrog integration scheme. Individual particle time steps τ are chosen to satisfy the criterium $\tau \lesssim \eta(\epsilon/a)^{1/2}$, where ϵ is the force softening length of a particle, a the magnitude of the local acceleration and η a constant determined on the basis of stability and accuracy requirements (for these runs $\eta = 0.2$). In order to maintain synchronization of the system, the time steps are quantized on power-of-two subdivisions of the largest time step (the "system" time step τ_s), i.e. $\tau \equiv \tau_n = \tau_s/2^n$ (e.g., Hernquist & Katz 1989). For these runs, 500–1000 system steps are used, equally spaced in time.

Here we consider two simulations of the cluster (the same object as in G98) with largely different resolutions, which we label LORES and HIRES. In the high resolution region of the box, the particle mass is $4.3 \times 10^8 h^{-1} M_\odot$ for LORES and $5.37 \times 10^7 h^{-1} M_\odot$ for HIRES; the softening is 1 and $0.5\,h^{-1}$kpc respectively. At the final epoch, the cluster has a radius $R_{200} = 1.0\,h^{-1}$Mpc (R_{200} is the radius within which the average density is 200 times the cosmic density and it is a measure of the extent of the virialized region) and a mass within such radius $M_{200} = 2.15 \times 10^{14} h^{-1} M_\odot$. With these parameters, run HIRES has more than 4 million particles within R_{200}, a factor of 8 of improvement with respect to LORES.

The mass growth curve of this cluster is shown in Figure 3 of Ghigna *et al* (1998). The cluster does not undergo major mergers since $z = 0.5$; the virial mass increases by $\lesssim$30% since that epoch, while the mass within the physical volume of the $z = 0$ cluster (i.e. the mass within $R < R_{200}|_{z=0}$) grows by only $\sim 10\%$. The early formation and "quiet" recent history of the cluster are convenient for this study, since they allows us to single out the effects of tides from major accretion or merger events. The results presented here are very likely typical of observed well relaxed clusters, but cannot be easily generalized to objects with more turbulent recent histories.

3. Halo substructure and its identification

The wealth of substructure that exists within the cluster is exemplified by Figure 1. The panels show maps of the projected density distribution in a box of side $2R_{200}$ for LORES (upper) and HIRES (lower panel). Each particle is plotted using a grey scale according to the logarithm of the local density (defined using an SPH smoothing kernel over 64 neighbouring particles using the code *SMOOTH* of Stadel & Quinn 1997, http ref: http://www–hpcc.astro.washington.edu/tools). Only regions with density contrast $\delta > 30$ are shown. The change of resolution from LORES to HIRES has a dramatic effect on the abundance of substructure: lower mass objects are resolved throughout the cluster and features appear in the very central region which was previously smooth.

The density maps are obtained at redshift $z = 0.5$, at which epoch more than 80% of the mass of the cluster is in place, yet it is not fully relaxed. In Figure 1, we can see three dominant substructure clumps (center, north, south-west). Similar features are observed in the light and X-ray distribution of observed high-redshift clusters (e.g. Abell 521; Maurogordato *et al* 2000). By $z = 0$, the second largest clump merges with the central object, the dark counterpart of a cD galaxy. At $z = 0.5$, the cluster's radius and masses are $0.6\,h^{-1}$Mpc (physical units) and $1.7 \times 10^{14} h^{-1} M_{\odot}$.

Identifying the substructure halos is a critical step (G98, KGKK). Here we use the group finding algorithm SKID, developed by Stadel *et al* (for a full description of the code see http://www–hpcc.astro.washington.edu/tools). SKID is a "Lagrangian" version of DENMAX (Gelb & Bertschinger 1994), the densities being evaluated at each particle position using an SPH smoothing kernel rather than at the nodes of a grid. The particles are moved along the density gradients until each oscillates around a point. They are then linked using a friends-of-friends algorithm (FOF; Davis *et al* 1985) and the groups (halos) found are checked iteratively for self-boundness.

In G98 we have verified the efficiency of SKID and tested the robustness of its estimates of the halo structural parameters (see below) against alternative methods. The ability of SKID to single out particles bound to substructure from the diffuse particles bound solely to the entire cluster (smooth background particles) depends crucially on the linking length, l_{FOF}, adopted for the FOF stage. If l_{FOF} is too small a subhalo will be fragmented into smaller units whereas if it is too large then halos will be merged together. A value $l_{FOF} \simeq 1/3 r_{peak}$, where r_{peak} is the distance from the halo's center at which the circular velocity profile has its peak v_{peak} (see, e.g., G98, section 3.3), is usually satisfactory. In our simulations, the subhalos have a large range of sizes and there is not a value for l_{FOF} that is ideal for all of them at a time; moreover there are many instances of substructure halos that contain their own substructure – "halos within halos within halos". To account for the complete hierarchy of substructure present in the current simulation we run SKID with three values of $l_{FOF} = 1.5$, 5 and $10\,l_{soft}$, and combine the outputs avoiding duplication. (SKID run with $l = 10 l_{soft}$ provides the first level of the "hierarchy" of halos; we then add the second level obtained with $l = 5 l_{soft}$ but discarding those halos that are separated from a first-level halo by a distance less than the latter's r_{peak}; and so forth for the third level. The completeness of the final halo catalog in several regions of the cluster was verified against the density concentrations visible in the 3D density map). However, it turns out that for the statistics of intermediate-to-massive halos (e.g. those with circular velocities larger than $\sim 100\,\mathrm{km\,s^{-1}}$) a run of SKID with $l_{FOF} = 10 l_{soft}$ is adequate (and fast).

We consider halos with a minimum number of member particles of 16 (corresponding to a mass of $8.6 \cdot 10^8 h^{-1} M_{\odot}$ in HIRES). In general, we use halos with more than 16 particles when they are employed as tracers, but we adopt a minimum number of 32 particles when their individual properties are relevant. The high resolution region analyzed is roughly the final turn-around radius, about twice the virial radius. Within this region, in HIRES, we identify over 2000 substructure halos. Within R_{200}, there are ~ 1200 halos at the final epoch and ~ 1000 at $z = 0.5$. The innermost halo is at $45\,h^{-1}$kpc from the cluster's center although about ten halos lie within a projected distance of $45\,h^{-1}$kpc.

We use the output of SKID to determine the halo structural parameters: radius r_{halo}, mass M_{halo} and "circular velocity" v_{circ} (the latter

is the peak value of the rotation curve $v(r) = (M(r)/r)^{1/2}$, where $M(r)$ is the halo mass within a distance r from its center). In § 4.1 of G98, we discussed the effects of numerical resolution on the completeness of subhalo samples. We modelled the substructure halos as isothermal spheres embedded in a larger isothermal potential — the cluster's halo — and used the standard formula for tidal stripping by the cluster's potential to estimate the limiting radii (tidal stripping is the main cause of subhalo disruption, once the cluster is in place). (Using NFW profiles to model the halos would not change our estimates significantly; see KGKK for a semi-analytical calculation using NFW profiles). Applying this simple model to the present simulation indicates that the halo samples obtained from LORES and HIRES should not be affected by major incompleteness for substructure halos with $v_{circ} \gtrsim 100$ and $60\,\mathrm{km\,s^{-1}}$, respectively, assuming pericenters greater than $50\,h^{-1}$kpc. We take these values as *quasi-completeness limits* of the subhalo samples; they mark the values of v_{circ} below which the samples become apparently incomplete. These estimates do not take into account halo disruption at redshifts $z > 1$, before the cluster is assembled. For instance, following the cluster's progenitors from high redshift to the present shows that the sample derived from HIRES may be $\sim 20\%$ incomplete starting from $v_{circ} \sim 100\,\mathrm{km\,s^{-1}}$ (see § 7).

4. The density profile of isolated halos

One of the most fundamental properties of dark matter halos is their global density profile. N-body simulations have been extensively used to study the structure of cold dark matter halos, yielding a variety of important results (e.g. Quinn *et al* 1986, Frenk *et al* 1988, Dubinsky & Carlberg 1991, Carlberg 1994, Navarro, Frenk & White 1996, 1997, Cole & Lacey 1996, Tormen, Bouchet & White 1996, Fukushige & Makino 1997, Brainerd *et al* 1998, G98, Tormen, Diaferio & Syer 1998, Huss, Jain & Steinmetz 1999, KGKK, Okamoto & Habe 1999). Systematic studies of halos across a wide range of masses has revealed a remarkable one parameter scaling (NFW profile; Navarro, Frenk & White 1996, 1997), with a density profile of the form $\rho(r) \propto r^{-1}(1 + r/r_s)^{-2}$, where $\rho(r)$ is the spherically-averaged density at the distance r from the halo's center and r_s a scale radius. The halos studied by NFW had $\approx 10^4$ particles within their virial radii and were resolved to a scale of a few % of this region. Moore *et al* (1998, 1999b) showed that increasing the resolution by about an order of magnitude produces steeper central cusps, $\rho(r) \propto r^{-1.5}$. Is the current resolution sufficient to resolve the central density profile of CDM halos or will increasing the resolution make the cusp even steeper?

Figure 2 shows the density profile of the cluster, measured in three runs with different resolutions — $\sim 10^{4.5}, 10^{5.7}$ and $10^{6.6}$ particles within the final virial radius. The lower solid curve shows the expected NFW curve for a halo of this mass in this cosmology. It provides a good fit to our lowest resolution simulation but underestimates the central density of the higher resolution runs. The upper solid curve shows the slightly modified profile proposed by Moore *et al* (1999; henceforth M99a), $\rho(r) \propto [(r/r_s)^{1.5}(1 + (r/r_s)^{1.5})]^{-1}$, where r_s is a scale radius. With increasing resolution, the cluster's profile appears to converge (asymptotically) to M99a's curve. The asymptotic profile is attained in the regions that have many particles and beyond several softening lengths; as it is shown by the vertical bars, density profiles measured from these N-body simulations can be "trusted" only for scales $\gtrsim$6 times the force resolution. This statement is likely to apply to simulations run with different techniques, provided force and mass resolutions are well balanced, but a detailed study of a large number of halos systematically varying the numerical parameters, time-stepping criteria etc, would be necessary to establish this (see also Moore, Katz & Lake 1996 and Moore *et al* 1998).

With increasing resolution, the profiles of substructure halos become closer to those of isolated halos. Figure 3 compares the "typical" profile of subhalos with $v_{circ} \sim 200\,\mathrm{km\,s^{-1}}$ in LORES and HIRES (obtained for each run by averaging the profiles of three subhalos with $R \sim 0.5R_{200}$ and v_{circ} close to $200\,\mathrm{km\,s^{-1}}$) with the profile of a similar isolated halo, simulated with 10^6 particles (data taken from Moore *et al* 1999). It is interesting to note that the typical subhalo profile is steeper in LORES than in HIRES, perhaps as a result of numerical relaxation between the hot halo particles and cold subhalo particles. This confirms that caution is required when studying the properties of the profiles of substructure halos even in

high-resolution simulations (G98; Avila-Reese *et al* 1999, Bullock *et al* 1999).

In a recent paper, Jing & Suto (1999) claim that the central density profiles of four simulated CDM clusters are closer to -1.1 than -1.5 as found here. We suspect that this difference may be due to the resolution. Jing etal use a Plummer softening with quoted resolution $0.005r_{200}$ (their Figure 2) and they measure the central slopes using the data between $0.007 < r/r_{vir} < 0.02$. This region may be dominated by dynamics on scales of order the softening (as seen above, we find that the profiles are reliable at scales that are 3 times the scale at which the force becomes Newtonian – our spline softening is completely Newtonian at twice the quoted values whereas a Plummer softening is still "softer" than Newtonian at the resolution quoted by Jing & Suto). It should be noted that a steep central profile (with $\rho(r) \propto\sim -1.4$) was also found by Moore *et al* 1998 using a high resolution simulation of a different cluster (the "Coma" cluster). At the resolutions achieved here and in Jing etal, only a handful of systems have been studied and the same cluster has not been simulated using different codes. We have placed our initial conditions on our website (www.nbody.net) so that other researchers can run this cluster and compare with the results presented here and in Ghigna *et al* (1998).

5. The substructure of dark matter halos

5.1. Distribution of circular velocities

The "circular" velocities v_{circ} of the subhalos are the quantities that can be most easily compared with observations (although the relation between v_{circ} and the rotation curve or velocity dispersion of the visible component of a galaxy is not straightforward; e.g. Navarro, Frenk & White 1996). Tidal truncation usually changes the mass of a halo by a large amount (often by $\sim$ 80-90%), however the peak circular velocity is a fairly stable quantity and can be regarded, to some extent, as a "label" that can identify a halo for several billion years within the cluster environment.

Major or total halo disruption is significant for those few massive halos (with $v_{circ} \gtrsim 400\,\mathrm{km\,s^{-1}}$) that take part in the formation of the cluster and undergo similar-mass mergers during the early phases of the assemblage, at $z \sim 2$ (see § 7); once the cluster is in place, the dynamical friction timescale is much larger than a Hubble time even for halos with mass $\sim 10^{13} M_{\odot}$ (for recent analyses on dynamical friction see van den Bosch *et al* 1999 and Colpi, Mayer & Governato 1999). Most of the substructure halos with small to intermediate masses survive within the cluster. On average, their central masses (the mass within r_{peak}) do not change dramatically and v_{circ} varies only as the cubed root of the mass. Over 5 billion years, v_{circ} varies by $\sim$ 20% and mainly for halos that spend a large fraction of their orbital period in the inner region of the cluster (G98, KGKK; see also below). Furthermore, since mergers are rare in clusters (G98, Okamoto & Habe 1999), most halos conserve their identities. This fact is useful, for example, to compare the v_{circ} distribution of a cluster's substructure halos with that of their progenitors predicted using the Press-Schechter (PS) approximation.

The differential velocity distribution function (VDF), defined as the number of halos per unit velocity interval per unit (physical) volume, is shown in Figures 4 and 5. The first Figure shows the effect of changing resolution. It compares the curves obtained for HIRES (solid line) and LORES (dotted) at the final epoch ($z = 0$, upper panel) and for the young cluster ($z = 0.5$, lower panel). We have used all the halos contained within the virial radius, R_{200}, at the two epochs, 0.975 and $0.6\,h^{-1}$Mpc respectively. The fall off at the low-velocity end are caused by incompleteness due to limited resolution, which dominates HIRES and LORES samples for $v_{circ} < 60\,\mathrm{km\,s^{-1}}$ and $< 100\,\mathrm{km\,s^{-1}}$, respectively. LORES's curve appears to be slightly affected by resolution up to $v_{circ} \sim 150\,\mathrm{km\,s^{-1}}$; beyond that v_{circ}, the results for the two runs agree well. In that range, the VDF at $z = 0$ is reasonably well approximated by a power-law with exponent -4, motivated by the PS approximation for field halos in this mass range (e.g. Gross *et al* 1998, Tormen 1998, Jenkins *et al* 1999; Klypin *et al* 1999b).

In order to single out evolutionary effects, we compare directly the halo distributions for run HIRES at the two epochs in Figure 5. In the main panel of the figure, we compare the VDFs measured for the halos within the *same physical (or proper) volume*, as determined by the virial radius of the cluster at $z = 0$. There is virtu-

ally no difference between the curves for the two redshifts (solid and dashed curves); the VDF is essentially "frozen" in time. We find the same result for the *normalized* VDFs, that is, the VDFs obtained considering only the subhalos within R200 at each respective epoch and measuring circular velocities and distances in units of the cluster's circular velocity and virial radius, also at the respective epoch; the comparison of the two curves is shown in the inset of the figure. (For these plots, we only show data for v_{circ} greater than the quasi-completeness limit of HIRES.)

The amplitude of the VDF of the subhalos (those within 0.3-0.5R_{200}) decreases a little over time, corresponding to a decrement of v_{circ} of about 20%. Tidal stripping removes particles orbiting at the outskirts of substructure halos but tidal heating of the halo cores, from tidal shocks near pericenter or from halo-halo encounters may also affect their concentrations and accelerate particles to the halo boundaries. A 20% decrement of v_{circ} corresponds to a $\sim$ 50% decrement of the mass. This effect may be physical but can be enhanced by limited resolution. In fact, the LORES simulation exhibits excessive mass loss of the inner halos with medium-to-small masses if compared with HIRES (see next section). KGKK have examined the central mass loss of a model subhalo of $v_{circ} \sim 200\,\mathrm{km\,s^{-1}}$, orbiting in a rich cluster with pericenter $\sim 150\,h^{-1}$kpc, varying the mass and spatial resolution (see their § 2.4). The halo's central mass loss depends on the force softening used, if the latter exceeds a certain "optimal" value ($\sim$ 1/30 of the halo's tidal radius at pericenter, for a Plummer softening; interestingly, the dependance on the particle mass is very weak); however, beyond the "optimal" resolution, the time evolution of the central mass appears to converge to a step function which drops by 20-30% at every passage at pericenter, yielding a mass loss of $\sim$ 50% over 5 billion years (the orbital period in their model is 2 Gyrs). In the HIRES simulation, the "optimal" resolution indicated by KGKK's test is met e.g. by subhalos of $v_{circ} \sim 100\,\mathrm{km\,s^{-1}}$ at $r_{peri} \sim 70\,h^{-1}$kpc and subhalos of $v_{circ} \sim 200\,\mathrm{km\,s^{-1}}$ at $r_{peri} \sim 50\,h^{-1}$kpc (we use the isothermal model approximation described in § 3 to obtain these estimates). The fractions of inner subhalos with $v_{circ} = 100$ and $200\,\mathrm{km\,s^{-1}}$ and with estimated pericenters less than $70\,h^{-1}$kpc and $50\,h^{-1}$kpc respectively are $\sim$ 20% in both cases; therefore the decrease of the VDF from $z = 0.5$ to $z = 0$ may be affected by numerical resolution, but, since the corresponding mass loss is close to the value expected from KGKK's test, it is probably a physical effect. In any case, it sets an upper limit. (For comparison, in LORES, the "optimal" resolution for $r_{peri} \sim 70\,h^{-1}$kpc is met only if $v_{circ} \gtrsim 200\,\mathrm{km\,s^{-1}}$).

The shape of the VDF does not depend significantly on the environment. This is also shown by Figure 5, where we plot the VDF for the inner subhalos ($R/R_{200} < 0.5$; upper dotted line) and those in the cluster's periphery ($1 < R/R_{200} < 2.5$; lower dotted line). A power-law $dN/dv_{circ} \propto v_{circ}^{-4}$ is always a reasonable fit for $v_{circ} \gtrsim 100\,\mathrm{km\,s^{-1}}$.

5.2. Mass distribution function

Knowledge of the mass distribution function (MDF) is useful to estimate the disruptive power of halo-halo collisions in dense environments. For example, modelling this process is necessary to understand the origin of intracluster light and the morphological evolution of galaxies in clusters and groups ("galaxy harassment"; Moore *et al* 1996). The mass and radii of substructure halos can also be probed directly using mass-reconstruction methods based on observations of arcs and arclets in clusters (Natarajan *et al* 1998).

The MDF provides information independent of that derived from the VDF. The mass of a halo of given v_{circ} depends on its orbital history, which determines the extent of tidal disruption that it has suffered. This strongly correlates with the smallest pericentric distance reached by a halo (G98) and, to a lesser degree, with the number of orbits completed (since a halo loses mass very quickly the first time it passes through pericenter and more slowly every time it completes an orbit; KGKK). However, since halos of different masses but with the same pericenter lose similar fractions of mass and the distribution of pericenters does not depend significantly on mass (G98), we still have roughly $M_{halo} \propto v_{circ}^3$, even for the subhalos.

Figure 6 plots the MDF for the substructure halos (defined as the number of halos per unit logarithmic mass interval per unit physical volume). Results are shown for both runs at the two redshifts considered previously. At $z = 0.5$, the agree-

ment between HIRES and LORES is good. The mass limit for which both runs are close to completeness (in the circular velocity distribution) is $\gtrsim 5.6 \cdot 10^{10} h^{-1} M_\odot$, the typical value for a halo with $v_{circ} = 100\,\mathrm{km\,s^{-1}}$ (see Figure 20 of G98). At $z = 0$, the MDF for the LORES cluster is $\sim 50\%$ lower than for the HIRES simulations. This difference, as for the VDF, is caused by numerically enhanced mass loss near the cluster's center; it disappears if we exclude the halos in the central region, $R/R_{200} < 1/2$, from the counts (Figure 7). As discussed in the previous section, our HIRES run is not affected significantly by artificial mass loss for $v_{circ} \gtrsim 100\,\mathrm{km\,s^{-1}}$, i.e $M \gtrsim 6 \cdot 10^{10} h^{-1} M_\odot$.

As found for the VDF, the MDF does not exhibit significant evolution within a physical volume during the lifetime of the cluster (Figure 8, main panel). At both redshifts, the MDF is close to a power-law $d\,n(M)/d\,M \propto M^{-2}$, for $M_{halo} \gtrsim 10^{11} h^{-1} M_\odot$, but becomes shallower for lower masses, $d\,n(M)/d\,M \propto M^{-1.7}$ (in the figure, we plot $dn/dLog_{10}M$). The main panel of Figure 8 also shows the MDF for inner and outer halos (symbols as for Figure 5); all the curves are similar, with slopes varying between -0.8 and -0.9. The inset shows the normalized MDFs for the cluster subhalos at the two redshifts, obtained in a similar way as the normalized VDFs of Figure 5 in the previous section.

The mass bound to substructure halos is a little more than 10% of the total cluster mass, with more fractional mass in halos at early rather than at late epochs. The value varies very slowly with resolution, but it can oscillate significantly since a large fraction of the mass belongs to the two or three most massive subhalos ($v_{circ} \sim 400 - 500\,\mathrm{km\,s^{-1}}$) that contribute $\approx 5\%$. If they are close to the cluster's center or if they possess their own substructure, the masses measured by SKID are quite sensitive to the linking length used and can differ significantly from estimates obtained adopting the spherical overdensity method (see G98), sometimes by a factor of 2. For instance, using the spherical overdensity method for LORES we find a global fraction of mass in subhalos of $\sim 13\%$ (G98), while using SKID's masses this value reduces to $\sim 11\%$. If we exclude the largest substructure halos, different mass estimates yield halo mass fractions differing only by about 1%.

Figure 9 plots the fraction of cluster mass that is in subhalos with circular velocity above a given value v_{circ}, but below $400\,\mathrm{km\,s^{-1}}$ The difference between the two runs never exceeds 1%. Also, between $z = 0.5$ and $z = 0$, the mass fraction decreases by only $\sim 1\%$ (note that the mass fraction is computed relative to the virial mass, M_{200}, at the respective epoch, namely 1.7 and $2.15 \times 10^{14} h^{-1} M_\odot$). Where the halo samples are close to completeness, the results are well represented by the function $M_{halos}(v_{circ} > \bar{v}_{circ})/M_{200} \simeq -0.09 \log_{10}[\bar{v}_{circ}/(\,\mathrm{km\,s^{-1}})] + \beta$, with $\beta = 0.23$-0.22. The mass fraction varies roughly linearly with clustercentric distance (G98, Figure 11).

5.3. The spatial distribution of substructure halos

In this section, we examine the bias existing between the spatial distribution of particles (i.e., the mass) and that of the subhalos. Here, the bias is defined as the ratio $b(R) \equiv n_{hal}(R)/n_{part}(R)$, where $n_{hal}(R)$ and $n_{part}(R)$ are the number density profiles of subhalos and particles as functions of clustercentric distance R. For convenience we normalize all quantities to the cluster parameters, i.e. we measure lengths in units of the virial radius, R_{200}, and N_{hal} and N_{part} as fractions of the total numbers of subhalos and particles within R_{200}. The halo distribution will be (positively) biased if $b(R)$ increases as R decreases, anti-biased in the opposite case. In G98 we found that the halos are anti-biased; Colín *et al* (1999) also find anti-bias for dark matter halos in large volume simulations of four cosmological models (they measure the bias defined by the ratio between the 2-point correlation functions of mass and dark matter halos, as it is customary for large scale structure studies). To study this problem it is particularly important to pay attention to the limitations imposed by the finite resolution, since overmerging — preferentially erasing subhalos in the central regions of the cluster — always introduces anti-bias in the subhalo distribution (or enhances it).

We compare the *normalized* (or fractional) number density profiles of halos and particles as a function of clustercentric distance R in Figure 10, for the redshifts $z = 0.5$ and $z = 0$ (top and bottom panel respectively). We plot the numbers of halos with $v_{circ} > v_{circ}^{LIM}$ in spherical shells of radius R divided by the volume of the shell (in units of R_{200}), divided by the total number

(N_{200}) of cluster subhalos above the circular velocity limit (the "cluster" subhalos are those contained in R_{200} at the respective epoch; this yields 188 and 219 subhalos if $v_{circ}^{LIM} = 80\,\mathrm{km\,s^{-1}}$, and 104 and 110 if $v_{circ}^{LIM} = 100\,\mathrm{km\,s^{-1}}$ for HIRES, while for LORES the corresponding numbers are 165 and 158, and 116 and 100). For the mass, we plot the particle number density profile divided by the number of particles within R_{200}. In each panel, the *long dashed* curves are the normalized mass profiles; the two other curves are for the halos of HIRES (*solid with errobars*) and LORES (*dotted*). For $z = 0.5$, we set $v_{circ}^{LIM} = 80\,\mathrm{km\,s^{-1}}$, which yield good statistics; for $z = 0$ we use $v_{circ}^{LIM} = 100\,\mathrm{km\,s^{-1}}$, which has similarly good statistics. Varying the value of v_{circ}^{LIM} does not make any difference, as long as there are enough halos to obtain significant measures.

Within the cluster, at $z = 0.5$, the halos have a number density profile similar to that of the mass, but the latter profile declines more steeply than the former approaching the virial radius and beyond (i.e., $b(R < R_{200}) < b(R > R_{200})$. This means that the population of halos (for a circular velocity limited sample) in the volume encompassing the cluster is globally anti-biased – with proportionally fewer halos where the particles are more clustered. At $z = 0$, there is also anti-bias, the mass being clearly more concentrated than the halos; for $R \sim 10\%$ of R_{200}, there is a factor of 2 of difference between the two profiles (and is even larger if we require that the two profiles overlap beyond R_{200}). At both redshifts, there are no significant differences between the curves for HIRES and LORES. Therefore the halo number density profiles measured from this simulation should not be significantly affected by residual overmerging (see also § 6).

Figure 11 compares directly the halo number density profiles at $z = 0.5$ and $z = 0$ in the physical (proper) volume centered on the cluster (for both samples, we set $v_{circ}^{LIM} \equiv 80\,\mathrm{km\,s^{-1}}$). The halos are clearly more concentrated in the volume of the newly formed cluster. Infalling material subsequently enhances the halo number density in the outer region, $R \gtrsim 600\,h^{-1}\mathrm{kpc}$ (the virial radius of the cluster at $z = 0.5$), while tidal disruption in the inner region reduces the number density of halos with circular velocities above the limit. It is interesting to note that allowing for a $\sim 20\%$ decrease of a halo's v_{circ} between $z = 0.5$ and $z = 0$ (because of central mass loss, as observed in the VDF analysis in § 5.3) is sufficient to recover most of the central steepness of the $z = 0.5$ profile; this is shown by the dotted line in the Figure. This indicates that, once the cluster is in place, tidal mass loss alone (instead of total halo evaporation) causes the measured decrement of the subhalo number density towards the cluster's center.

Apart from tidal mass loss, mergers between halos during the cluster assembly (at $z > 0.5$) are probably a major cause of the anti-bias between halos and particles. At $z = 0.5$, the uniform anti-bias of the cluster subhalos (with respect to the 'field'; as seen in Figure 10, upper panel) may reflect the fact that the cluster has only recently being assembled through the merging of group-sized halos of similar masses, so that mergers and tides have affected its subhalo population more uniformly. Note that the galaxies that would reside in the subhalos could have a different bias, if their circular velocities are not directly affected by the central mass loss of their dark halos. As a final word of caution, we point out that the issue of bias would be better addressed with a statistical sample of clusters and a more representative sample of field halos. This approach requires a trade-off between statistics and resolution but considerable progress has recently been made (Colín *et al* 1999; see also Kauffmann *et al* 1999a,b, Diaferio *et al* 1999, Benson *et al* 2000).

5.4. Velocities of halos and dark particles

The issue of velocity bias — the difference between galaxy and dark matter (DM) velocities — was first addressed by Carlberg & Couchmann (1989) as a means of reconciling low measures of Ω from the observed velocities of galaxies in clusters. There are two types of velocity bias considered in the literature, the one-point velocity bias ($b_v = \sigma_{V,halos}/\sigma_{V,DM}$) which compares the velocity dispersions of galaxies and dark matter particles (e.g. Carlberg & Dubinski 1991, Carlberg 1994) and the two-point or pairwise velocity bias ($b_{v,12}$) which compares the relative velocity dispersions in pairs of objects (e.g. Couchmann & Carlberg 1992). Here we consider the first type. A recent paper (Colín, Klypin & Kravtsov 1999; CKK hereafter) focussed on the different forms of velocity bias for numerical simulations of the ΛCDM

cosmology. The situation is still rather confusing. CKK find that the dark matter halos within clusters are positively biased, with $b_v \sim 1.2$-1.3 (similar results were also found by Diaferio *et al* 1998 and Okamoto & Habe 1999), while KGKK find $b_v \lesssim 1$ for a similar set of data (see their Figure 15). In G98, we did not detect velocity bias. The difference may be partly due to the fact that G98 and KGKK measure the global b_v using the whole sample of cluster subhalos, while CKK consider the radial profile $b_v(R)$. We re-examine the issue here in more detail. Note that the comparison between the spatial distribution of the halos and that of the mass considered in the previous section, does not provide sufficient information, since the scaled profiles of differently biased tracers may not differ much (Carlberg 1994).

We compare the 3D velocity dispersion ($\sigma_{V,3D}$) profiles of halos and dark matter for run HIRES in Figure 12 (the averages are taken in spherical shells of width $250\,h^{-1}$kpc; at the center, $\sigma_{V,3D}$ for the DM drops sharply from $\sim 1300\,\mathrm{km\,s^{-1}}$ at $R \sim 50\,h^{-1}$kpc to $1000\,\mathrm{km\,s^{-1}}$ at $R \sim 10\,h^{-1}$kpc, if radial bins of width $10\,h^{-1}$kpc are used, as it is shown by the light solid curve in the lower panel of the figure). We consider the cluster at $z = 0$ (lower panel) and also the output at $z = 0.1$, separated in time from the final epoch by less than one typical subhalo orbital period; we also subdivide the halos in three subsamples according to the values of their circular velocities (as listed in the figure). In this way, we should be able to single out significant differences between the (3D) velocities of halos and dark matter from statistical flukes, partly overcoming the drawback of dealing with only one cluster. The samples with $v_{circ} > 150\,\mathrm{km\,s^{-1}}$ have the worst statistics, especially for $R > R_{200}$ where they provide ~ 5 halos per bin.

With quite large oscillations, the $\sigma_{V,3D}$ of the halos is consistent with that of the dark matter for $R \gtrsim 300\,h^{-1}$kpc. Within the cluster, the data show a significant (positive) bias in the innermost bin, with $b_v = 1.2$-1.3. The maximum amplitude of bias in our data is similar to that reported by CKK but the signal is globally weaker (CKK have $b_v \simeq 1.2$ at $R/R_{200} \simeq 0.7$, that is $\gtrsim 600\,h^{-1}$kpc for the cluster studied here). We also show the velocity dispersion profiles of halos and particles for run LORES, in Figure 13. The trend of increasing b_v with decreasing R is more apparent in this case. Here, the sample with the lowest circular velocities is largely incomplete due to limited resolution; interestingly, it exhibits a more marked bias than the other samples. It is also interesting to note that there are no obvious biases in the distribution of the orbital parameters of the halos and the particles (we have computed the orbits approximating the cluster potential to a static spherical potential obtained from its density profile, as in G98, § 4.6).

When we average over the virial volume of the cluster, the velocity bias of the halos in the central region has a small impact; in the three cases considered previously, the global bias within R_{200} is always less than 1.1 (although it remains positive). Also considering only massive halos ($v_{circ} > 200\,\mathrm{km\,s^{-1}}$) does not yield any significant bias. In this case, anti-bias would be expected if dynamical friction were efficient in slowing down such halos, but the friction time for subhalos within a cluster is almost always larger than the Hubble time (see Colpi, Mayer & Governato 1999 for a recent analysis). Even restricting the samples to half the virial radius does not make a significant difference (in one case, for HIRES at $z = 0.1$, there is anti-bias, but the other two yield positive or no bias, unless the "cD≡global potential" is included).

In conclusion, we find evidence of positive velocity bias in the central region of the cluster but the signal is much weaker than CKK's detection. It seems that limited resolution enhances the signal; overmerging accentuates the impact of physical processes like mergers and total halo disruption that could lead to positive velocity bias. A larger set of high-resolution simulations would be welcome to address these issues with better statistics.

6. Survival of substructure halos

As seen in § 5, over the lifetime of the cluster the abundance of substructure does not appear to change significantly; however substructure is erased also at earlier redshifts. To examine this issue, we have identified the dark matter halos that are progenitors of the cluster at $z = 1$ and $z = 3$ (using the public friends-of-friends code available from http://www–hpcc.astro.washington.edu/tools, run with a linking length of 0.2 times the mean interparticle separation). We define as progeni-

Fig. 1.— Maps of the cluster's density as seen in run LORES (upper panel) and HIRES, which has 8 times better mass resolution. The change in the appearance between the two runs is mainly due to HIRES's ability of resolving further down the substructure mass function.

$v_{circ,\,min}$	N_{halos}	p_{traced}	p_{cD}
$230\,\mathrm{km\,s^{-1}}$	15	90%	$\sim 10\%$
$100\,\mathrm{km\,s^{-1}}$	120	100%	0%
$50\,\mathrm{km\,s^{-1}}$	550	82%	0%

Table 1: Results of tracing the cluster's progenitor halos at $z = 1$ to the substructure halos at the final time (*descendents*), for three ranges of mass of the progenitors (corresponding to more than $10,000$, between $10,000$ and $1,000$, and between $1,000$ and 100 particles). The first and second columns report the minimum circular velocity of the progenitors in each mass range and their number; the third and fourth columns give, respectively, the percentage of progenitors in each range with a descendent at $z = 0$ other than the "cD" object, and the percentage of progenitors that merge with the "cD". (These values are obtained requiring for the descendents a minimum number of traced particles $N_{p,min}$ equal to 1% of the particles in the progenitor and not less than 4; there is no difference if we set $N_{p,min}$ to be at least 16).

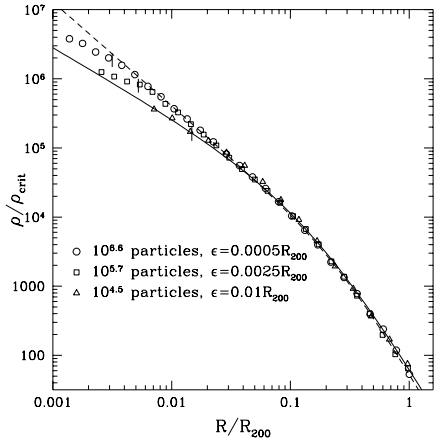

Fig. 2.— The density profile of the cluster measured in three runs with increasing resolutions (from triangles to squares to circles). In the best run, the cluster contains over 4 million particles and the force resolution is 0.05% of the cluster's virial radius. The curves are an NFW profile (lower curve) and a fit with the profile of Moore *et al* (1999a), which rises more steeply ($\propto r^{-1.5}$) at the center than the NFW profile ($\propto r^{-1}$). With increasing resolution, the cluster's profile continues to approach M99a's curve *i.e.* this appears to be the asymptotic profile in the limit of infinite resolution. The vertical bars mark the radii at which the measured profiles are no longer affected by finite numerical resolution.

$v_{circ,\,min}$	N_{halos}	p_{traced}	p_{cD}
$300\,\mathrm{km\,s^{-1}}$	23	40% (40)	60% (60)
$150\,\mathrm{km\,s^{-1}}$	180	90% (90)	10% (7)
$70\,\mathrm{km\,s^{-1}}$	1070	70% (61)	3% (0.1)

Table 2: Results of tracing the cluster's progenitor halos at $z = 3$ to the substructure halos at the final time. The mass ranges and the quantities in the columns are the same as in table 1 (in the last two columns, the values in brackets give the percentages obtained requiring $N_{p,min}$ to be at least 16).

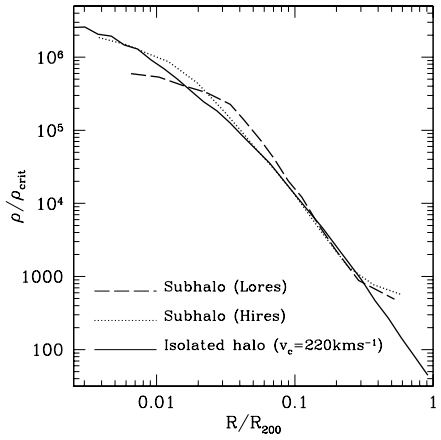

Fig. 3.— The typical density profile of a substructure halo with $v_{circ} \sim 200\,\mathrm{km\,s^{-1}}$ (and cluster-centric distance $\sim 0.5\,R_{200}$) in the two runs, compared with the profile of an isolated halo (simulated with much higher resolution). Increasing the resolution brings the profiles of substructure halos closer to those of their isolated counterparts.

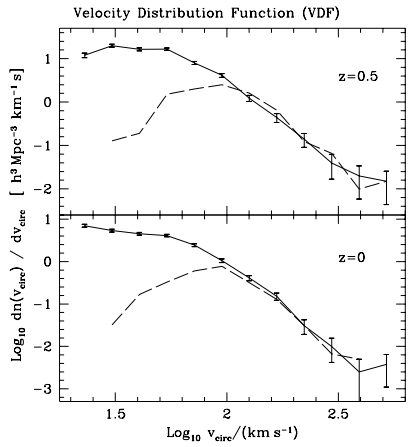

Fig. 4.— Velocity distribution function (VDF) of the substructure halos, at two redshifts (lower panel: the final epoch, $z = 0$; upper panel: the young cluster at $z = 0.5$, when it is ~ 1 billion years old). The figure shows the effect of increasing the resolution by a factor of 8 in mass (from LORES, dashed curve, to HIRES, solid curve). The errorbars represent (1-σ) Poisson errors on the counts. The curves agree well where we expect both runs to be close to completeness (roughly $v_{circ} > 100\,\mathrm{km\,s^{-1}}$). The fall off at the low velocity end is caused by finite numerical resolution.

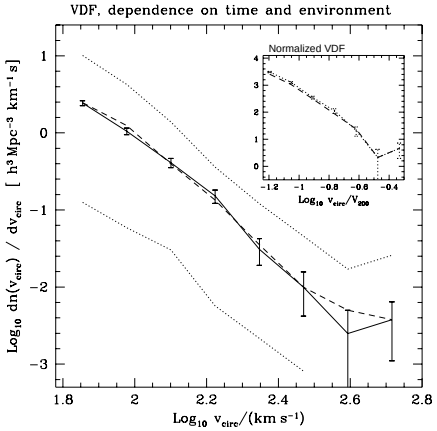

Fig. 5.— The VDF for the cluster's substructure halos at $z = 0$ (solid line) compared with that of the halos at $z = 0.5$ contained within the same physical volume (dashed), using in both cases $R_{200}|_{z=0}$ as limiting distance (main panel). The inset shows the VDFs obtained considering only the halos within the cluster's virial radius at $z = 0$ (dashed) and $z = 0.5$ (dotted) and and measuring v_{circ} in units of the cluster's "circular velocity" at the respective epoch. In both cases, there are no significant changes in the shape and amplitude of the VDF during the lifetime of the cluster. The two dotted curves in the main panel show the effect of changing environment inside and around the evolved cluster ($z = 0$); they are for inner subhalos ($R/R_{200} < 0.5$; upper curve) and "peripheral" halos ($1 < R/R_{200} < 2.5$; lower). Within and around the cluster the shape of the VDF is very similar.

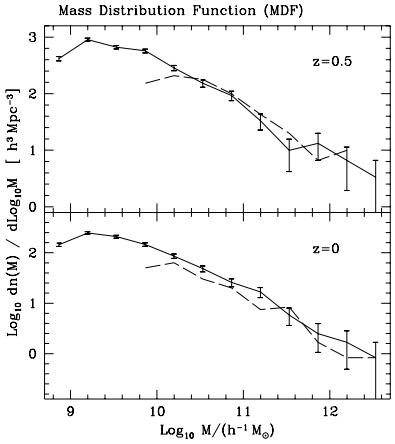

Fig. 6.— The mass distribution function (MDF) of substructure halos at two redhifts (lower panel: $z = 0$; upper panel: $z = 0.5$) for the two runs (LORES, dashed curve; HIRES, solid curve). The errorbars are (1-σ) Poisson errors on the counts. As for the VDF, at $z = 0.5$, the curves agree well where we expect both runs to be close to completeness ($M \gtrsim 5.6 \cdot 10^{10} h^{-1} M_{\odot}$). At $z = 0$, the deficiency of LORES's MDF is due to numerically enhanced mass loss of medium to small mass halos in the central region (see Figure 7).

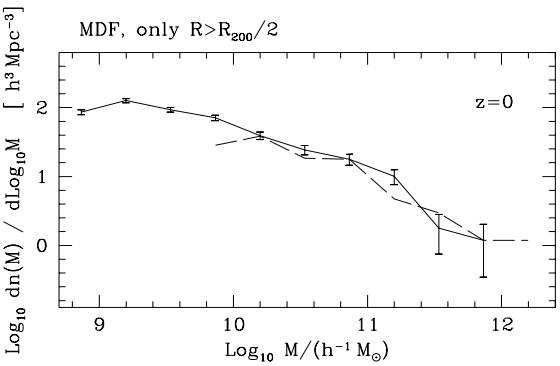

Fig. 7.— Same as in the lower panel of Figure 6, but here the halo samples have been constructed requiring $R > 1/2 R_{200}$. The curves for HIRES (solid) and LORES (dashed) are close in this case.

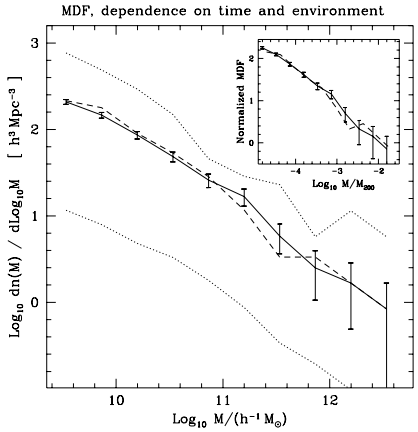

Fig. 8.— Main panel: the MDF at $z = 0$ for the cluster's halos (solid line, HIRES data) compared with that of the halos at $z = 0.5$ contained in the same physical volume (dashed line; the curves are shown only in the range where they are not significantly affected by resolution). The mass function is "frozen in time" and its shape does not depend much on the environment either, as it can be seen by considering only the inner subhalos ($R/R_{200} < 0.5$; upper dotted curve, main panel) or those in the "periphery" ($1 < R/R_{200} < 2.5$; lower dotted curve, main panel). The inset shows the normalized MDFs at the two redshifts, obtained in a similar way as the normalized VDFs of Figure 5.

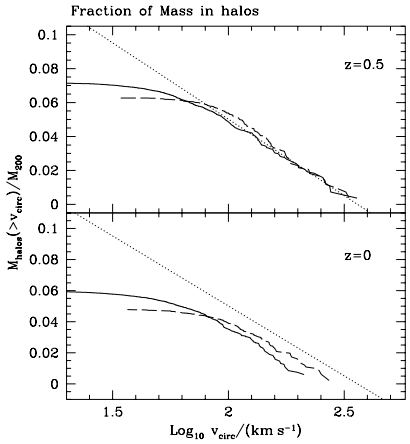

Fig. 9.— Fraction of cluster mass bound to subhalos with circular velocities exceeding a given value v_{circ}, at $z = 0.5$ (upper panel) and $z = 0$ (lower), for HIRES (solid line) and LORES (dashed). We also set an upper limit of $400\,\mathrm{km\,s^{-1}}$ to exclude the most massive halos whose masses have a relatively large scatter; they contribute alone an additional $\sim 5\%$. The light dotted line is a fit to the $z = 0.5$ curves for $v_{circ} > 100\,\mathrm{km\,s^{-1}}$ (the flattening of the curves at the low-velocity end is due to the incompleteness of the samples). The bound mass fraction is $\propto \log(v_{circ})$, thus varies slowly with resolution.

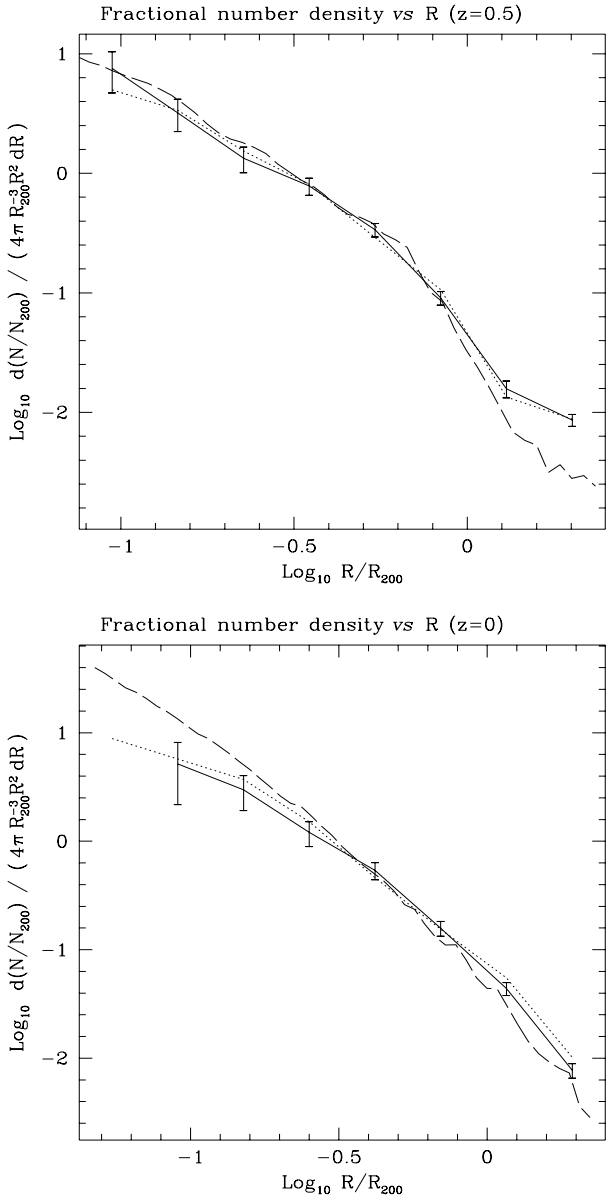

Fig. 10.— Fractional number density of halos and particles as a function of clustercentric distance R, at $z = 0.5$ (upper panel) and $z = 0$ (lower panel); lengths are in units of the virial radius R_{200} at the respective epoch; N_{200} is the number of halos or particles within R_{200}. In the top panel, the solid curve (with 1-σ Poisson errobars) is for HIRES's subhalos with $v_{circ} > 80\,\mathrm{km\,s^{-1}}$; the dotted curve is LORES's equivalent. The dashed line is the particle (i.e. the mass) profile. The subhalos are always antibiased with respect to the mass, although at $z = 0.5$ their profile is similar to that of the mass within the cluster.

tors those halos that contribute particles to the virial volume of the cluster at the final epoch. We have then "traced" them to the substructure halos identified at $z = 0$, by comparing the indexes of their particles. For the $z = 0$ subhalos we use only the 'core' particles, *i.e.* those that are separated from the halo centers by a distance less than the value of r_{peak} - this (conservative) approach avoids ambiguities when there is a hierarchy of substructure. For the central object, we adopt a radius $r_{cD} = 25\,h^{-1}$kpc, a value that should single out the progenitor halos that merge to form the "cD" core against those that only supply particles to its halo through tidal stripping.

We accept descendents only if they have a number of traced particles larger than 1% of the particles of the progenitors and not less than a minimum number, $N_{p,min}$, which we varied between 4 and 16 (the number of particles traced can be small for small halos since we only consider their 'core' particles). In our approach, a progenitor with no descendent subhalos at $z = 0$ should have been completely disrupted with its particles lost in the diffuse particle background of the cluster or, possibly, in the outer parts of large subhalos (visual inspection of 10 cases confirms this). Such halos may survive if the numerical resolution were increased further, so that the fraction of progenitors with no descendents is an estimate of the importance of residual numerical effects. Cases in which two or more progenitors have a common descendent, i.e. the progenitors' particles contribute to the descendent's core, point to true mergers.

Table 1 reports the results of the tracing for the $z = 1$ progenitors in three mass ranges. Table 2 is the analog for $z = 3$. In the first column, we show the minimum value of the circular velocity for the progenitors in each mass range. All the $z = 1$ progenitors with $v_{circ} > 100\,\mathrm{km\,s^{-1}}$ have a descendent at $z = 0$; the tracing is still essentially complete at $v_{circ} \gtrsim 70\,\mathrm{km\,s^{-1}}$ ($p_{traced} = 98\%$) and deteriorates only for v_{circ} approaching $50\,\mathrm{km\,s^{-1}}$ ($p_{traced} \simeq 80\%$). The central object accretes only another halo (of $v_{circ} \sim 300\,\mathrm{km\,s^{-1}}$). These results are stable against varying N_{min}. The loss of halos from $z \sim 1$ to the present appears negligible for $v_{circ} > 100\,\mathrm{km\,s^{-1}}$.

The most prominent feature of the tracing of the $z = 3$ progenitors is the large fraction of massive halos that merge with the central object: about 25 progenitors with $v_{circ} > 150$, a dozen for $v_{circ} > 300\,\mathrm{km\,s^{-1}}$. There is virtually no contribution to the central object's (core) mass from progenitors with $v_{circ} < 150$. Essentially all the progenitors with $v_{circ} > 150\,\mathrm{km\,s^{-1}}$ have a partner at $z = 0$; the tracing starts deteriorating at $v_{circ} \lesssim 100\,\mathrm{km\,s^{-1}}$ where the percentage of "childless" progenitors is 18%, independent of N_{min} in the range 4-16. Successful tracing with the "cD" might still hide overmerging, but it seems safe to consider the mergers of the massive halos as real, since they occur before the cluster formation and involve objects of comparable masses (for which the dynamical friction time is small). Also the distribution of their particles in the $z = 0$ cluster is well concentrated within the cD. We have examined the distribution at the final epoch of the particles in the cores of the $z = 3$ progenitors with $v_{circ} > 200\,\mathrm{km\,s^{-1}}$ that merge with the cD (we use $r_{core} = 20$ kpc comoving); about 80% of such particles end up within $50\,h^{-1}$kpc from the cluster's center at $z = 0$. Very likely further increases of resolution, and the inclusion of baryons with cooling, will reveal substructure within a cD's radius; e.g. the substructure already present within the progenitors at $z = 3$ could survive and be found within the cD. However, these subhalos would lose a very large fraction of their masses and should have small circular velocities and low mass-to-light ratios.

In conclusion, overmerging effects in this simulation appear negligible for large and intermediate halos; loss of substructure may still affect halos starting from $v_{circ} \sim 100\,\mathrm{km\,s^{-1}}$ at the $\sim$20% level. This does not seem to be important for most of the statistical properties of the substructure considered in the previous section, in view of the strict similarities of the results for LORES and HIRES (except possibly for the velocity bias).

7. Summary and Conclusions

We use "N-body" simulations to follow the collisionless evolution of the dark matter component of a rich galaxy cluster. Increasing the force and mass resolution (Figure 1) by an order of magnitude has a dramatic effect on the abundance of substructure and allows us to assess the biases introduced by low resolution studies. We find the following main results:

- We compare the density profile of the cluster halo simulated with 2×10^4, 6×10^5 and 4×10^6 particles within the virial radius. At our highest resolution the force softening is $0.5\,h^{-1}$kpc (0.05% of the virial radius) and the profile is well fit by $\rho(r) \propto [(r/r_s)^{1.5}(1+(r/r_s)^{1.5})]^{-1}$. This agrees with the results of Moore *et al* (1999b) for lower resolution simulations, and suggests that we may have converged on the asymptotic central slope. The best fit NFW profile to the data has residuals of order 30%. (In a recent paper, Jing & Suto, 2000, find shallower central cusps ($\rho(r) \propto r^{-1.1}$) for four high resolution simulations of clusters in the ΛCDM model; the reasons of the disagreement are not yet clear, see § 4).

- For the first time we can confidently resolve the cluster density profile beyond $\approx 0.2\% R_{vir} = 2\,h^{-1}$kpc. Between $2\,h^{-1}$kpc and $40\,h^{-1}$kpc the density profile has a central cusp with a slope $\rho(r) \propto r^{-1.5} \pm 0.05$. This disagrees with the central mass profile of CL0024+1654 recovered from a strong lensing analysis which indicate a constant density core over the same radial range (Tyson *et al* 1998).

- The density profiles of substructure halos has not yet "converged". Lower resolution studies found that halos within clusters had steeper density profiles than field halos – this may be due to particle-halo heating of substructure halos.

- The distribution function of substructure circular velocities (VDF) is essentially invariant over the lifetime of the cluster (~ 5 billion years) and is quite close to a power-law $dn(v_{circ})/dv_{circ} \propto v^{-4}$, with little dependence on environment (§ 5.1). Clusters simulated with $\sim 10^6$ particles can reliably measure this function for halos with circular velocity above $100\,\mathrm{km\,s^{-1}}$. (Note that the cluster forms early, at $z \gtrsim 0.5$, with no major mergers since; the evolution of the properties of the substructure may be different in objects with more turbulent recent histories.)

- The distribution of halo masses (MDF) shows the same "invariance properties" as the VDF –virtually no evolution and little dependence on environment– and is close to a power-law $dn/dM \propto M^{-2}$ for halo masses $\gtrsim 10^{11} h^{-1} M_\odot$ (a fraction 5×10^{-4} of the cluster's virial mass); tidally driven mass loss changes the MDF self-similarly (§ 5.2). Clusters simulated with $\sim 10^6$ particles can reliably measure this function for halos with masses above $6 \times 10^{11} h^{-1} M_\odot$.

- The substructure halos of circular velocity limited samples are spatially anti-biased with respect to the underlying mass distribution (see § 5.3 for definitions). At an early epoch ($z = 0.5$), the anti-bias is uniform within the cluster (halo and particles have number density profiles of similar shape); at the final time, the anti-bias of the halos increases approaching the cluster's center. Halo-halo collisions and tidal mass loss (which decrease a halo's v_{circ}, on average by $\sim 20\%$ over 5 billion years) are the likely source of the anti-bias (§ 5.3).

- The 3D velocity dispersions of halos and dark matter particles are generally consistent within and around the cluster, except in the central region ($R < 0.3 R_{200} = 300\,h^{-1}$kpc) where the halos are "hotter" than the particles with a (positive) velocity bias $b_v \equiv \sigma_{v,halos}/\sigma_{v,DM} = 1.2$-$1.3$). The sign and maximum amplitude of the bias is similar to that reported by Colín *et al* (1999), but the radial range over which $b_v > 1$ is much more limited (their detection extends to $R \sim 0.8 R_{200}$). The magnitude of the bias appears to be enhanced by limited resolution since "overmerging" erases preferentially the central cluster halos. When we average over R_{200}, the velocity dispersions of halos and particles do not differ by more than 10%.

- Following the cluster progenitors from high redshift to the present shows that, at the current resolution, overmerging should be globally unimportant for subhalos with $v_{circ} \gtrsim 100\,\mathrm{km\,s^{-1}}$, although a fraction of high-redshift halos may be lost for v_{circ} close to $100\,\mathrm{km\,s^{-1}}$. All the cluster progenitors with $v_{circ} \gtrsim 70\,\mathrm{km\,s^{-1}}$ at $z = 1$ have a descendant among the subhalos at $z = 0$;

about 20% of the progenitors at $z = 3$ with $v_{circ} \sim 100\,\mathrm{km\,s^{-1}}$ may be artificially disrupted. The "cD" object at the cluster's center is assembled at high redshift ($z \sim 3$ to 1) through the merging/accretion of a dozen halos with $v_{circ} \lesssim 300\,\mathrm{km\,s^{-1}}$; it also accretes one large halo within the cluster (at $z < 0.5$).

It is now clear that the hierarchical model for structure formation can naturally form massive dark matter halos that contain a wealth of substructure resembling observed galaxy clusters; high resolution numerical simulations allow us to obtain robust statistical measures of the properties of the substructure and make detailed predictions. Since substructure halos are expected to host galaxies in a cluster and galaxy satellites in a galaxy, the comparison with the observed distribution of those objects can produce important tests for the cosmological models. For example, whereas the MDF obtained from cluster simulations in the CDM universe easily reproduces that derived from the observed circular velocity function of cluster galaxies (Moore *et al* 1999a), the predicted abundance of substructure of galactic halos is not matched by the observed population of satellites of the Milky Way and Andromeda (Klypin *et al* 1999b, Moore *et al* 1999a).

Acknowledgments

SG is a Marie Curie Fellow of the TMR program of the European Union (4-th framework, grant n. ERBFMBICT972103). We are grateful to Carlos Frenk, Volker Springel, Simon White and the referee for helpful comments and suggestions. The numerical simulations analysed here were performed using the Edinburgh Cray T3E supercomputer as part of the VIRGO consortium and partially on the SGI Origin at NCSA. Some of the analyses were carried out at the SGI Origin of the UK's National Cosmology Supercomputer COSMOS.

REFERENCES

AbdelSalam, H. M., Saha, P. & Williams, L. L. R. 1998, AJ, 116, 1541

Adami, C., Mazure, A., Katgert, P. & Biviano, A. 1998, A&A, 336, 63

Allen, S. W. 1998, MNRAS, 296, 392

Avila-Reese, V., Firmani C., Klypin A. & Kravtsov, A. V. 1999, MNRAS, 310, 527

Benson, A. J., Cole, S., Frenk, C. F., Baugh, C. M. & Lacey, C. G. 2000, MNRAS, 311, 793

Brainerd, T. G., Goldberg, D. M. & Villumsen, J. V. 1997, ApJ, 502 505

Bullock, J. S., Kolatt, T. S., Sigad, Y., Somerville, R. S., Kravtsov, A. V., Klypin, A., Primack, J. R. & Dekel, A. 1999, MNRAS, submitted (preprint astro-ph/9908159)

Carlberg, R. G. & Couchmann, H. M. P. 1989, ApJ, 340, 47

Carlberg, R. G. & Dubinski, J. 1991, ApJ, 340, 47

Carlberg, R. G. 1994, ApJ, 433, 468

Carlberg, R. G., Yee, H. K. C., Ellingson, E., Abraham, R., Gravel. P., Morris, S. & Pritchet, C. J. 1996, ApJ, 462, 32

Carlberg, R. G., Yee, H. K. C., Ellingson, E. 1997, ApJ, 478, 462

Cole, S. & Lacey, C. 1996, MNRAS, 281, 716

Colín, P., Klypin, A. & Kravtsov, A. V. 1999, ApJ, submitted (astro-ph/9907337)

Colín, P., Klypin, A., Kravtsov, A. V. & Khokhlov, M. 1999, ApJ, 523, 32

Colpi, M., Mayer, L. & Governato, F. 1999, ApJ, 525, 720

Couchmann, H. M. P. & Carlberg, R. G. 1992, ApJ, 389, 453

Davis, M., Efstathiou, G., Frenk, C.S. & White, S.D.M. 1985, ApJ 292, 371.

Diaferio, A., Kauffmann, G., Colberg, J. M. & White, S. D. M. 1999, MNRAS, 307, 537

Dubinski, J. & Carlberg, R. 1991, ApJ, 369, 13

Flores, R. A. & Primack, J. R. 1994, ApJ, 457, L5

Flores, R. A., Maller, A. H. & Primack, J. R. 2000, ApJ, 535, 555

Frenk, C. S., Evrard, A. E., White, S. D. M. & Summers, F. J. 1996, ApJ, 472, 460

Frenk, C. S., White, S. D. M., Davis, M. & Efstathiou, G. 1988, ApJ, 327, 507

Fukushige, T. & Makino, J. 1997, ApJ, 477, L9

Ghigna, S., Moore, B., Governato, F., Lake, G., Quinn, T. & Stadel, J. 1998, MNRAS, 300, 146.

Gelb, J. M. & Bertschinger, E. 1994, ApJ, 436, 467

Gross, M. A. K., Somerville, R. S., Primack, J. R., Holtzman, J. & Klypin, A. 1998, MNRAS, 301, 81

Hernquist, L. & Katz, N. 1989, ApJS, 70, 419

Huss, A., Jain, B. & Steinmetz, M. 1999, ApJ, 517, 64,

Jenkins, A., Frenk, C. S., Pearce, F. R., Thomas, P. A., Colberg, J. M., White, S. D. M., Couchman, H. M. P., Peacock, J. A., Efstathiou, G. & Nelson, A. H. 1999, ApJ, 499, 20

Jing, Y. P. & Suto, Y. 2000, ApJ, 529, 69

Kauffmann, G., Colberg, J. M., Diaferio, A. & White, S. D. M. 1999a, MNRAS, 303, 188

Kauffmann, G., Colberg, J. M., Diaferio, A. & White, S. D. M. 1999b, MNRAS, 307, 529

Klypin, A., Gottlöber, S., Kravtsov, A. & Khokhlov, M. 1999a, ApJ, 516, 530

Klypin, A., Kravtsov, A., Valenzuela, O. & Prada, F. 1999b, ApJ, 522, 82

Kneib, J-P., Ellis, R. S., Smail, I., Couch, W. J. & Sharples, R. M. 1996, ApJ, 503, 77

Markevitch, M., Vikhlinin, A., Forman, W. R. & Sarazin, C. L. 1999, ApJ, 527, 545

Maurogordato, S., Proust, D., Beers, T. C., Arnaud, M., Pello, R., Cappi, A., Slezak, E. & Kriessler, J. 2000, A&A, 355, 848

Meneghetti, M., Bolzonella, M., Bartelmann, M., Moscardini, L. & Tormen, G. 2000, MNRAS, 314, 338

Moore, B. 1994, *Nature*, 370, 620

Moore, B., Katz, N. & Lake, G. 1996, 456, 455

Moore, B., Governato, F., Quinn, T., Stadel, J. & Lake, G. 1998, ApJ, 499, 5

Moore, B., Ghigna S., Governato F., Lake, G., Quinn, T. Stadel, J. & Tozzi, P. 1999a, ApJL, 524, 19 (M99a)

Moore, B., Quinn, T., Governato F., Stadel, J. & Lake, G. 1999b, MNRAS, 310, 1147 (M99b)

Natarajan, P., Kneib, J. P., Smail, I. & Ellis, R. S. 1998, ApJ, 499, 600

Navarro, J. F., Frenk, C. S. & White, S. D. M. 1996, ApJ, 462, 563

Navarro, J. F., Frenk, C. S. & White, S. D. M. 1997, ApJ, 490, 493

Okamoto, T & Habe, A. 1999, ApJ, 516, 591

Press, W. H. & Schecter, P. 1974, ApJ, 187, 425

Quinn, T., Katz, L., Stadel, J. & Lake, G. (1997), preprint (astro–ph 9710043)

Smail, I., Ellis, R. S., Dressler, A., Couch, W. J., Oemler, A. Jr., Sharpless, R. M., Butcher, H. 1997, ApJ, 479, 70

Summers, F. J., Davis, M. & Evrard, A. E. 1995, ApJ, 454, 1

Tormen, G., Bouchet, F. R. & White, S. D. M 1996, MNRAS, 286, 865

Tormen, G. 1997, MNRAS, 290, 411

Tormen, G. 1998, MNRAS, 297, 648

Tormen, G., Diaferio, A. & Syer, D. 1998, MNRAS, 299, 728

Tyson, J.A., Kochanski, G.P. & Dell'Antonio, I.P. 1998, ApJL, 498, L107.

van den Bosch, F. C., Lewis, G. F., Lake, G. & Stadel, J. 1999, ApJ, 515, 50

White, S. D. M. & Rees, M. 1978, MNRAS, 183, 341

White, S. D. M., Davis M, Efstathiou, G. & Frenk, C. S. 1987, Nature, 330, 451

Williams, L. L. R., Navarro, J. F. & Bartelmann, M. 1999, ApJ, 527, 535

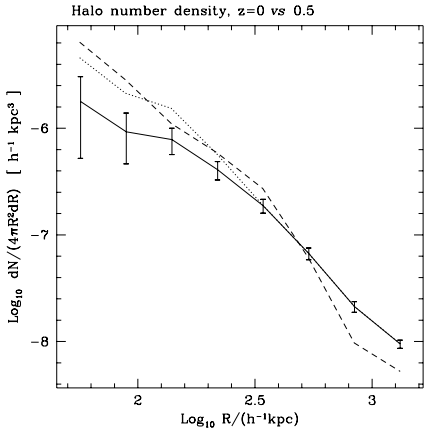

Fig. 11.— The number density profiles in physical (proper) volume using halos with $v_{circ} > v_{circ}^{LIM} \equiv 80\,\mathrm{km\,s^{-1}}$ at $z = 0$ (solid line) and $z = 0.5$ (dashed) . The halo number density decreases in the central region ($R \lesssim R_{200}/3$). The dotted line shows the effect of having a variable v_{circ}^{LIM} that drops by $\sim 20\%$ for $R < R_{200}/4$ (precisely, by 15% in the radial range $0.125 < R/R_{200} < 0.25$ and by 25% for $R/R_{200} < 0.125$).

This 2-column preprint was prepared with the AAS LaTeX macros v5.0.

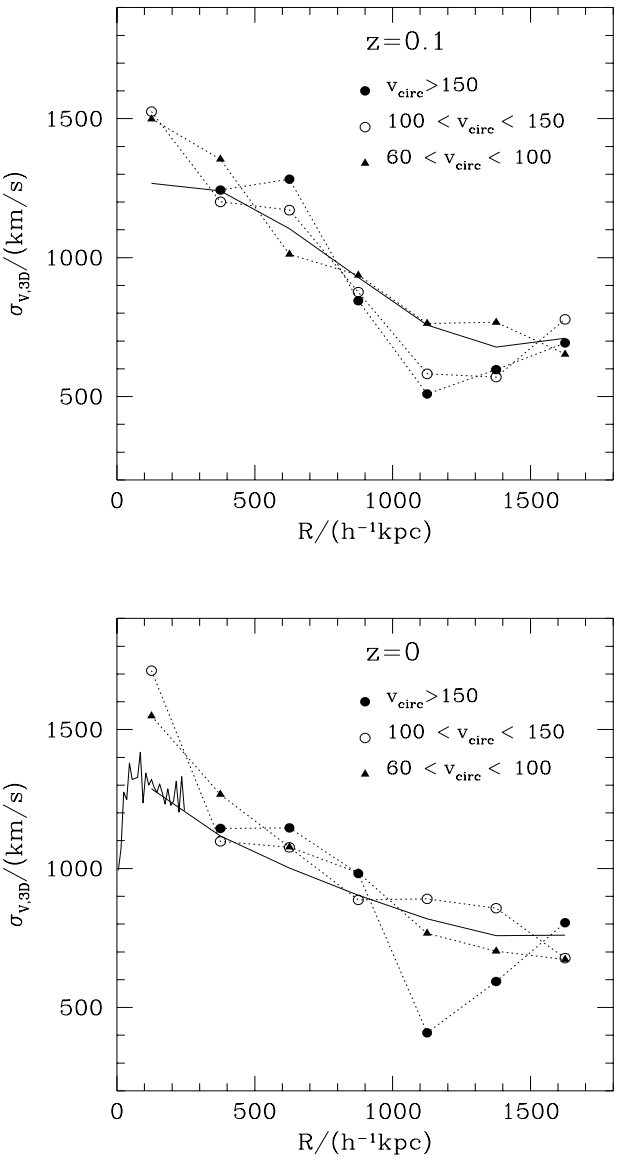

Fig. 12.— 3D velocity dispersion profiles for the dark matter (solid curve) and for three samples of halos (the points on the dotted curves) selected according to their circular velocities as outlined on the figure (v_{circ} in $\mathrm{km\,s^{-1}}$). The data are for HIRES at the redshifts $z = 0.1$ and $z = 0$; R_{200} is respectively $0.88\,h^{-1}$Mpc and $0.975\,h^{-1}$Mpc. (The curve for $v_{circ} > 150$ does not extend to the innermost bin, since the latter contains only two such halos - the "cD" has been excluded (it is always at rest since it simply the central smooth cluster potential; the profile for the dark matter using fine bins near the cluster's center is shown by the light solid line in the lower panel). The halos in the central region ($R \lesssim 300\,h^{-1}$kpc) are "hotter" than the DM, with $b_v \sim 1.2$-1.3.

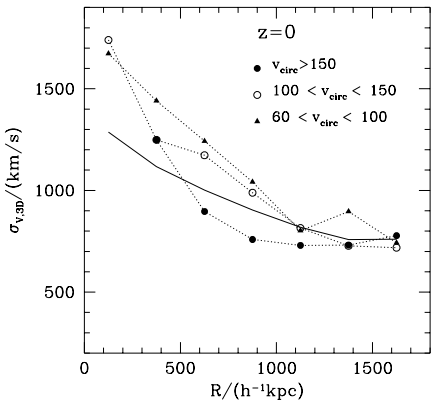

Fig. 13.— Same as in Figure 12 but using data from LORES at $z = 0$. The positive bias of the halos in the central region is more marked than for HIRES.